Accelerating Proton-Coupled Electron Transfer of Metal Hydrides in Catalyst Model Reactions

Authors: Tianfei Liu[1], Meiyuan Guo[1], Andreas Orthaber[1], Reiner Lomoth[1], Marcus Lundberg[1], Sascha Ott[1], Leif Hammarström[1]*

Affiliations:

[1]Department of Chemistry, Ångström Laboratory, Uppsala University, Box 532, SE-751 20 Uppsala, Sweden.

*Corresponding author. E-mail: Leif.Hammarstrom@kemi.uu.se

Abstract: **Metal hydrides are key intermediates in catalytic proton reduction and dihydrogen oxidation. There is currently much interest in appending proton relays near the metal center to accelerate catalysis by proton-coupled electron transfer (PCET). However, the elementary PCET steps, and the role of the proton relays, are still poorly understood, and direct kinetic studies of these processes are scarce. Herein, we report a series of tungsten hydride model complexes with covalently attached pyridyl groups as proton acceptors. The rate of their PCET reaction with external oxidants is increased by several orders of magnitude compared to that of the analogous systems with external pyridine, thanks to facilitated proton transfer. Moreover, the mechanism of the PCET reaction is altered by appending the bases. A unique feature is that the reaction can be tuned to follow three distinct PCET mechanisms, with very different sensitivities to oxidant and base strength. Such knowledge is crucial for rational improvements of solar fuels catalysts.**

The energy-efficient production of solar fuels [1-5], and their conversion into electricity in fuel cells [6,7], employ key principles of natural photosynthesis and respiration, and have engaged scientists for decades. At the molecular level, the formation and utilization of a solar fuel like hydrogen (H_2) involves multiple electron- (ET) and proton transfer (PT) steps. To avoid build-up of charge, the two processes are often inter-dependent, giving rise to proton-coupled electron transfer (PCET) reactions. These can proceed stepwise, one before the other, or in a concerted fashion where the proton and the electron transfer simultaneously. Inspired by many enzymes that demonstrate exquisite control on PCET reactions[8,9], the introduction of proton relays in the secondary coordination sphere of catalysts has become a popular strategy, aiming to facilitate protonation and deprotonation of metal-bound aqua species (M-OH/M-OH_2) [10,11], hydrides (M-H) [12-14] or carboxylates (M-CO_2) [15-18]. The exact mechanism by which the proton relays accelerate catalysis is often unclear, but implicitly assumed to be due to enhanced probability for proton tunneling. While being tempting, this assumption is far from obvious because of the multi-step nature of catalysis, which complicates kinetic analysis, and other factors that may dictate reaction rates. For example, the introduction of pendant proton relays in some transition metal catalysts for O_2 or CO_2 reduction caused large changes in the catalyst reduction potential, or led to facilitated substrate

binding, both of which may be mistaken for proton relay effects [15,19,20]. Also, while computational studies have provided valuable insight, it is in general difficult to determine if PCET occurs via a concerted or step-wise mechanism, e.g. for the much studied NiP_2N_2 catalysts [12,13,21]. For informed and effective catalyst design, it is imperative to disentangle these different phenomena and mechanistic pathways. In this context, we set out to directly measure the acceleration that a proton relay in the second coordination sphere of a metal-hydride (M-H) can provide during M-H oxidation[22,23]. This process is a PCET reaction and a key step in hydrogen oxidation chemistry (Fig. 1), as found for example in fuel cells, and its microscopic reverse is a key step in proton or carbon dioxide reduction to a fuel.

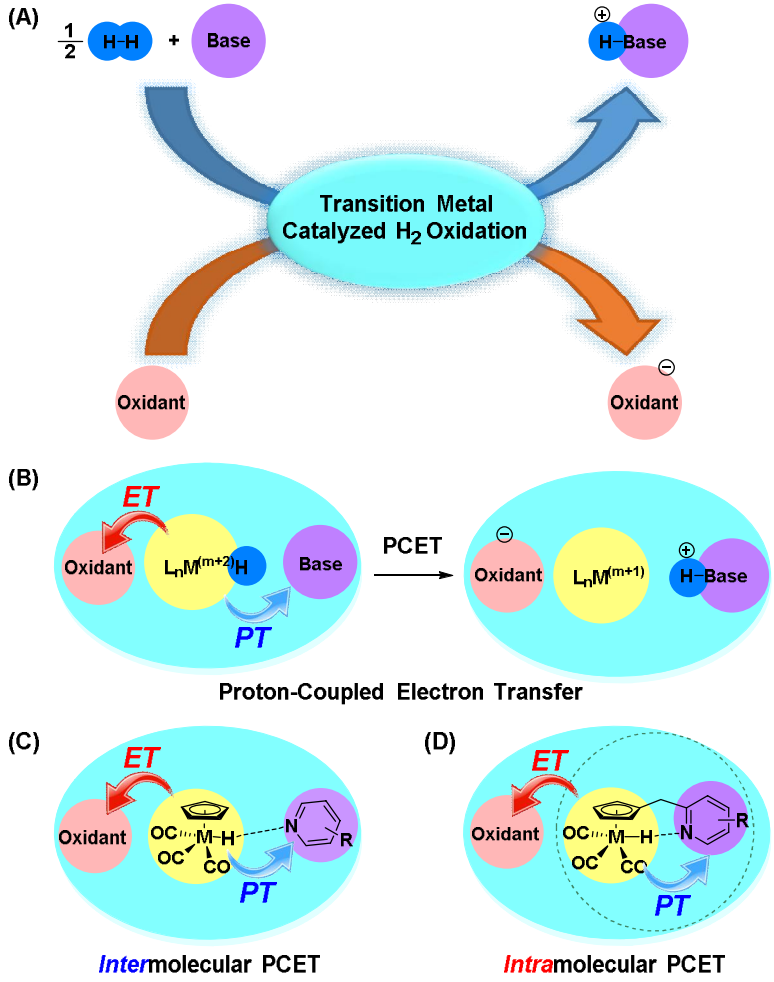

Figure 1. (A) Transition metal catalyzed H_2 oxidation; (B) the proton-coupled electron transfer (PCET) reaction on the key metal-hydride intermediate in most proposed mechanisms for transition metal catalyzed H_2 oxidation; (C) previous work on the concerted intermolecular PCET reaction of a tungsten-hydride complex[22]; (D) the intramolecular PCET reaction of tungsten-hydride complexes with pendant pyridyl groups in used this study.

Proton tunneling is a non-adiabatic process that is ignored in many theoretical treatments of enzymes and solid-state catalysts, which instead focus on the classical reaction barrier [24,25]. Yet, efficient proton tunneling may result in faster rates, beyond those predicted by scaling relationships that appear to place limits on practical catalytic activities [21,26]. Proton tunneling does not affect the thermodynamic potentials of chemical transformations, but may increase the reaction rate when PT is involved in the rate-determining step. This has for example been shown in phenolic model systems in which proton donor and acceptor distance and interaction largely dictate proton tunneling rates [27-30]. However, M-Hs are generally distinct from typical organic "Eigen acids"[31] (e.g. carboxylic acids, phenols or iminium groups) that have a tendency to form strong hydrogen bonds, have low intrinsic PT barriers, and are well studied for fundamental principles of PCET. Thus, only recently, we reported a first example of a concerted PCET from a metal-hydride, [CpWH(CO)$_3$] (Fig. 2A), to external based and oxidants (Fig. 1C)[22]. The concerted reaction proceeded directly to the products, W$^{\bullet}$ and H$^+$, without the formation of any intermediates such as W$^-$ or W-H$^+$ that would be formed in the step-wise mechanisms (Fig. 2B).

The reaction barrier for the concerted pathway is often lower than for the stepwise mechanisms (see below), making it ideal as rate-determining step in catalysis where a low overpotential is desirable. Our previous result was an important proof-of-principle that a concerted pathway can indeed be realized in M-Hs. Nevertheless, for this particular system the reaction rate was still rather slow. Our hypothesis was that the reaction could be accelerated by suitably appended base groups in the M-H complex. In the present study, we have therefore synthesized a series of cyclopentadienyl tungsten-hydride (W-H) complexes that are decorated with pyridine bases of different basicity in their second coordination spheres (**3a-e**; Fig. 3), from the reaction of the corresponding ligands **1a-e** with W(CO)$_6$ (**2**). By direct kinetic measurements of the elementary step (Fig.1D), we show that the rate of PCET can thus be increased by several orders of magnitude compared to the analogous systems with external pyridine.

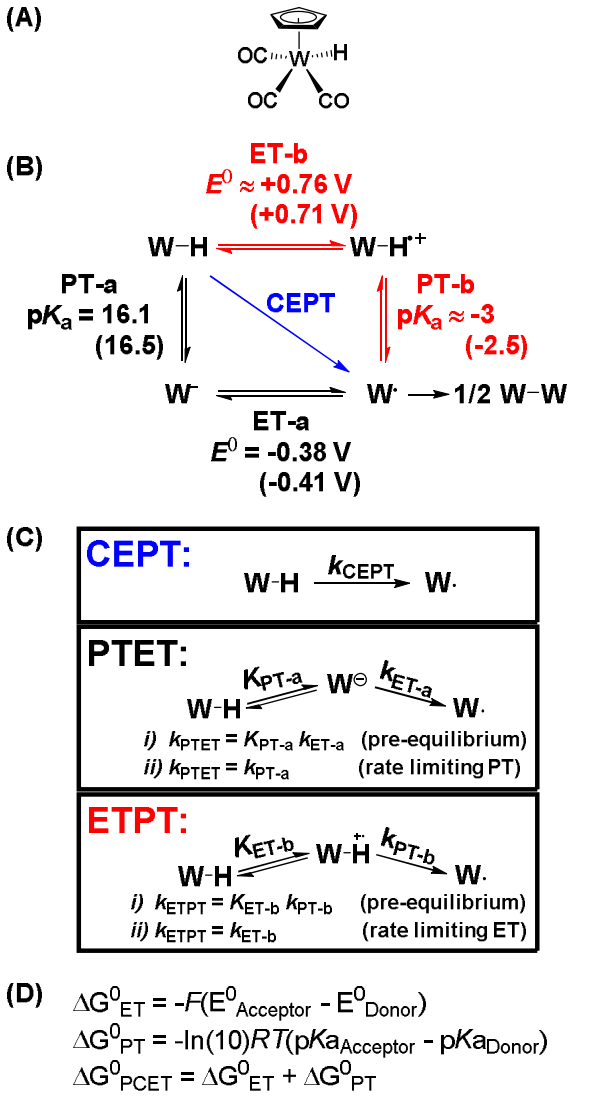

Figure 2. (A) Structure of [CpWH(CO)$_3$]. (**B-D**) Mechanistic and thermodynamic basis to analyze the reaction kinetics and its variation with strength of oxidant and base: (**B**) Mechanistic pathways for W-H oxidation[22]: stepwise PTET (pathway a, black), stepwise ETPT (pathway b, red), and concerted electron-proton transfer (CEPT) in a single kinetic step (pathway in blue). The thermodynamic data given are for the previously studied [CpWH(CO)$_3$] in CH_3CN (E^0 [32-34] vs. $Fc^{+/0}$ and pK_a [35,36]), with data for [(MeCp)WH(CO)$_3$] in brackets (this study). (**C**) Kinetics for the three pathways, with the two kinetic limits for the step-wise mechanisms: either pre-equilibrium conditions or a rate-limiting first step. (**D**) The free energy for the ET, PT and PCET steps of panel (B) can be estimated from the E^0 and pK_a values of the W-species relevant for each step, E^0 of the oxidants and pK_a of the pyridinium groups.

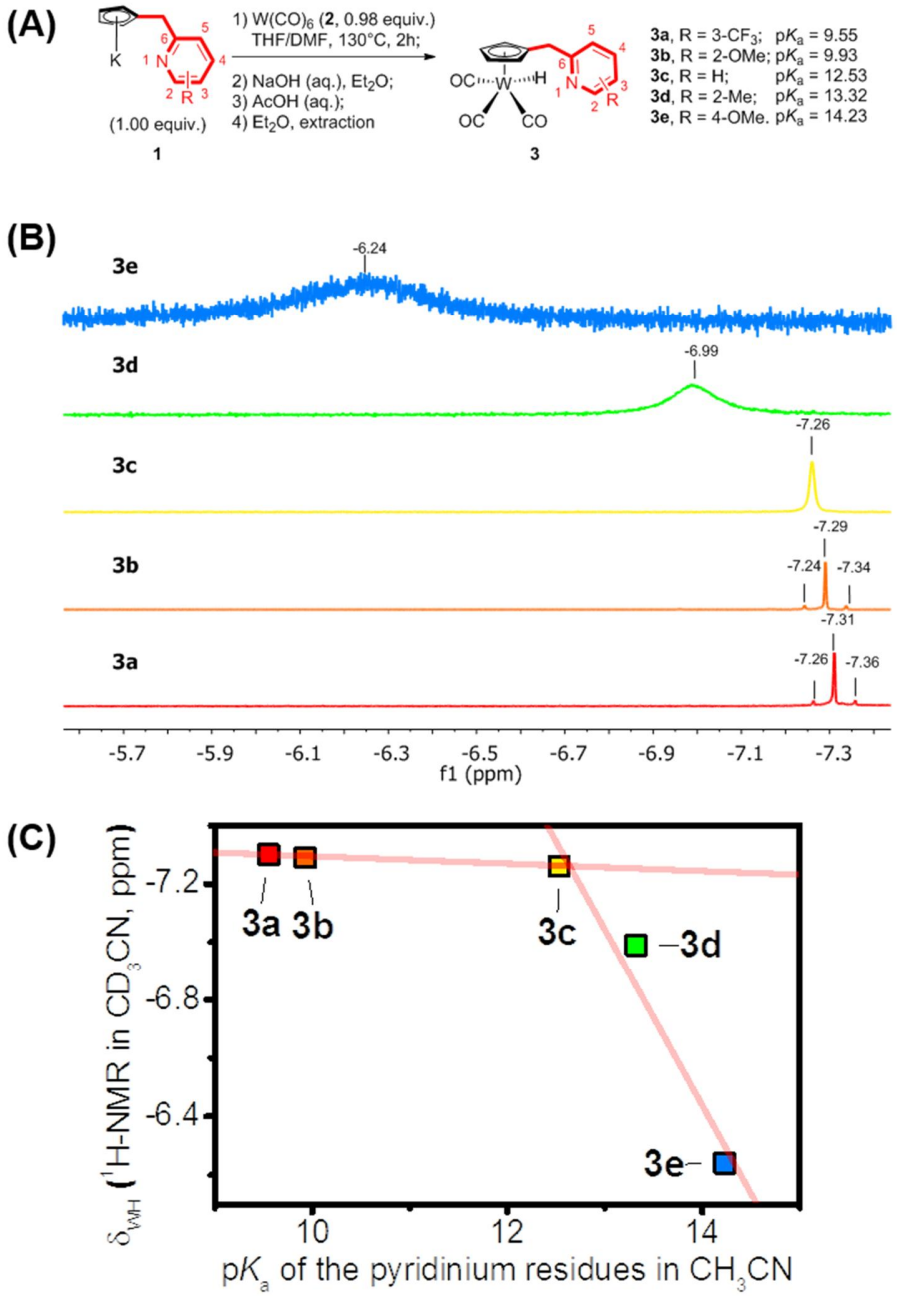

Figure 3. (**A**) The synthetic route of complexes **3,** and pK_a values in CH_3CN of the conjugate acids of the pyridine residues [37,38]. (**B**) ^{1}H-NMR spectra (CD_3CN) in the W-H region of complexes **3** at 25 °C; the broad signals for **3d** and **3e** have been multiplied by a factor of 10 and 100, respectively, to be visible in the plot, but the peak integral corresponds to one proton in each of the complexes. Color codes: **3a**, red; **3b**, orange; **3c**, yellow; **3d**, green; **3e**, blue. (**C**) plot of the δ_{WH} in complexes **3** at 25 °C versus pK_a of the corresponding pyridinium residue.

Mechanisms of PCET

Three possible mechanisms for PCET in **3a-e** should be considered (Fig. 2B). One is a stepwise, proton-first mechanism (PTET), where intramolecular proton transfer (PT-a) to yield the zwitterion [$W^{-\cdots+}$HPyR] is followed by outer-sphere electron transfer (ET-a). Another stepwise mechanism (ETPT) is electron transfer (ET-b) to generate the [W-$H^{+\bullet}\cdots$PyR] cation radical, followed by intramolecular proton transfer to the pyridyl group (PT-b). Finally, the third possibility is a concerted electron proton-transfer (CEPT) in a single kinetic step, where both electron and proton tunnel at the same transition state.

Eq. 1 is a general expression for the rate constant k_i for a single-step CEPT, ET or PT reaction (non-adiabatic limit) [21,26,39] where the pre-exponential factor A_i is proportional to the electron and/or proton tunneling probability, ΔG_i^0 is the reaction free energy and λ_i is the reorganization energy.

$$k_i = A_i \cdot exp\left[-\frac{\Delta G_i^{\#}}{RT}\right] \quad (1a)$$

$$\Delta G_i^{\#} = \frac{\left(\Delta G_i^0 + \lambda_i\right)^2}{4\lambda_i} \quad (1b)$$

The CEPT pathway is thermodynamically favored because it uses all the available free energy (Fig. 2D) in a single reaction step. In contrast, the initial steps of the ETPT and PTET are uphill, as seen from the E^0 and pK_a values for W-H (Fig. 2), the oxidants and pyridinium groups (Table 1). Thus, unless the initial PT-a or ET-b step has much smaller reorganization energy (λ) than CEPT, the activation free energy ($\Delta G^{\#}$) will be lower for the latter mechanism (eq. 1b). Note that the step-wise reactions can never be faster than their initial forward step, so a smaller driving force for the initial step will always be a disadvantage (at moderate driving force, $-\Delta G_i^0 < \lambda_i$). On the other hand, the tunneling probability of CEPT can be smaller because it involves both electron and proton. A balance between these two factors can often explain the competition between the mechanisms[22]. A strong oxidant tends to favor an ETPT mechanism, while a strong base favors PTET. If both oxidant and base are weak, the overall driving force is small, and CEPT is often the preferred mechanism. This gave us the possibility to tune the mechanism by using different oxidants and bases, as we had previously shown for tyrosine and tryptophan residues [29,40].

Results and Discussion

The complexes became available in acceptable isolated yields from the reaction of the corresponding ligands **1a-e** and $W(CO)_6$ (**2**), followed by protonation (Fig. 3A; see the Method section and the Supporting Information for details on the synthesis and characterization). The intramolecular H-bond between the W-H and the pyridines is not visible in the single crystal X-ray structures of **3a**, **3d** and **3e** due to unfavorable conformations caused by packing effects between pyridyl groups in the solid state (**SI**). Their presence in homogenous solution (CH_3CN) is clearly manifested through ^{1}H-NMR spectroscopic studies, and supported by theoretical analyses (see **SI**). The ^{1}H-NMR spectra of **3a** and **3b** show one sharp peak of W-H at -7.31 and -7.29 ppm, respectively with obvious ^{183}W-^{1}H satellites (Fig. 3B), implying that the intramolecular H-bond [W-H···PyR] in **3a** and **3b** is very weak. In the absence of a strong H-bond, conformations that arise from rotations around the W-Cp vector and the flexible CH_2 linker may be populated (**SI**). The ^{1}H-NMR spectra of **3c**-**3e** show resonances for the W-H proton that range from -7.26 ppm to -6.24 ppm, a downfield shift that is concurrent with a broadening of the peak. (Fig. 3B-3C). This is consistent with a stronger intramolecular H-bond [W-H···PyR] for the complexes with the stronger pyridine bases.

To evaluate the thermodynamics of PCET (Fig. 2D) the relevant pK_a (p. S19-S22) and E^0 values were determined (Fig. 2B, Table 1; see also SI). The cyclic voltammogram of $[(MeCp)WH(CO)_3]$ in acetonitrile showed an irreversible anodic peak at 0.71 V vs. Fc^+/Fc, ca. 50 mV lower than that observed for $[CpWH(CO)_3]$[22,32,34] due to the electron donating methyl substituent (Fig. 4A). In **3a-e** the first anodic peak appears at much lower potential, from -0.079 V to -0.326 V, because proton transfer to the appended pyridine base thermodynamically stabilizes the oxidized complex; *cf.* pK_a($W^{\cdot}H^+$) » -2.5 *vs.* pK_a(pyridinium) = 9.5–14.2. With a Nernstian dependence on this difference in pK_a, E_{peak} is predicted to shift cathodically by 0.99 V from $[(MeCp)WH(CO)_3]$ to **3e**, close to the experimentally observed shift of 1.04 V. Moreover, for **3a-e** E_{peak} shifts by 52 mV/pK_a unit of the pyridinium unit (Fig. 4B). This suggests that the PCET driving force ($-\Delta G^0_{PCET}$) increases as expected from the pyridine base strength, i.e. that the *relative* values of $-\Delta G^0_{PCET}$ in the series are well predicted from the pK_a values of the free pyridinium groups. While accurate relative values are sufficient for the correlations between rate constants and pK_a in Fig. 5, also the absolute ΔpK_a values for PT between the metal and pyridine in **3a-e** seems to be predicted within one unit, as suggested by the 6% W^-…H^+py form seen in the IR spectrum of **3e** (Fig. S45).

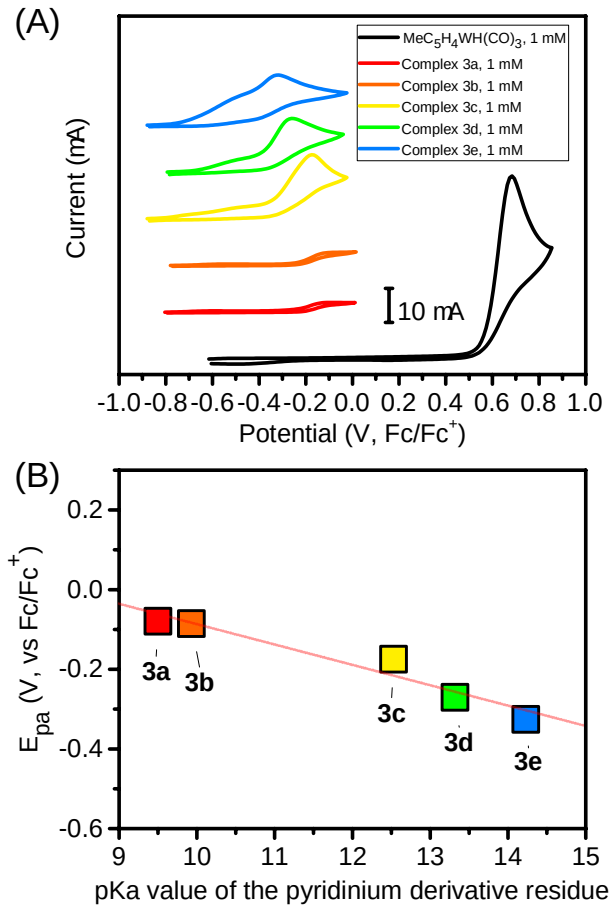

Figure 4. (**A**) Cyclic voltammetry of **3a-e** and [(MeCp)WH(CO)$_3$] in acetonitrile. The first anodic peak for [(MeCp)WH(CO)$_3$] appears at E_{peak} = +0.71 V vs. $Fc^{+/0}$ (for [CpWH(CO)$_3$] E_{peak} = +0.76[34]). The voltammetry of [CpWH(CO)$_3$] has been thoroughly investigated and the first oxidation has been attributed to formation of the [CpW(CO)$_3^{\cdot}$] radical, that undergoes rapid further oxidation and/or dimerization, depending on conditions (see ESI).[32,34] In **3a-e** the first anodic peak appears at much lower potential because proton transfer to the appended pyridine base thermodynamically stabilizes the oxidized complex. Similar effects have been show with addition of exogenous pyridines to [CpWH(CO)$_3$],[22] and for hydrogen-bonded phenols.[41] (**B**) A plot of E_{peak} for **3a-e** versus pK_a of the corresponding pyridinium residue (scan rate = 0.1 V/s). The straight line is a linear fit to the data with a slope of -52 mV/pK_a unit.

The kinetics of the elementary PCET reactions from complexes **3a-e** and $[M(R_2bpy)_3]^{3+}$ oxidants (M = Fe, Ru; R_2bpy = 4,4'-disubstituted 2,2'-bipyridines; Table 1) was measured in acetonitrile under argon at 25 °C using stopped-flow spectrophotometry (see Fig. S21-S34 for example traces). The data obtained was compared to that of the previously published $[CpWH(CO)_3]$[22] in the presence of exogenous pyridines. Second-order conditions were applied in all measurements ([**3a-e**] = [oxidant]), and the reduction of oxidant followed second-order kinetics with no significant variation in the rate constant for different initial concentrations (Fig. S26-S31). The product of the PCET step, $[W^{\bullet}\cdots H^{+}Py]$, can be expected to dimerize with near-diffusion controlled kinetics,[42] and our spectroscopic analysis demonstrated the good purity of both the reactants and the dimeric product (Fig. S17-S20). Together with additional control experiments (Fig. S15-S20) this shows that the kinetics is not significantly perturbed by any side reactions. The reaction was monitored by the absorbance at the wavelength maximum of the Fe^{II}/Ru^{II} visible band, where **3a-e** and the resulting dimer show only weak absorption (Fig. S16-S19).

The second order PCET rate constants (k_{obs}) determined for **3a-e** are given in Table 1. Fig. 5 compares the values for **3a-e** (colored symbols) with those for $[CpWH(CO)_3]$ and external pyridines reported before (black symbols)[22]. It is clear that k_{obs} is strongly accelerated when the pyridine base is appended in the 2nd coordination sphere (**3a-e**). The value of k_{obs} for the weakest oxidant $[Fe((MeO)_2bpy)_3]^{3+}$ with **3a-e** (colored squares, solid grey line) is much larger than with $[CpWH(CO)_3]$ and 3 mM external pyridines (black squares, purple dashed line), by a factor of nearly 100 to more than 10,000, depending on the pK_a of the pyridinium group. Also with the strongest oxidant $[Ru(Me_2bpy)_3]^{3+}$, k_{obs} is faster with **3a-d** (colored point-down triangles, purple solid line) than with $[CpWH(CO)_3]$ and external pyridines (black point-down triangles, red dashed line), by up to a few orders of magnitude. Moreover, the reaction of $[Fe((MeO)_2bpy)_3]^{3+}$ with either **3c** (100 mM) or an equimolar amount of the methylated reference compound $[(MeCp)WH(CO)_3]$ and pyridine (100 mM each) showed that **3c** reacted ca. 5000 times faster (Fig. S22). This is the first time that the acceleration of an elementary PCET reaction, caused by a second sphere effect of a metal complex, is measured in a direct kinetic experiment. The acceleration can obviously be very large, and is due to an increased probability of proton transfer. For **3c** the rate corresponds to that estimated for $[(MeCp)WH(CO)_3]$ at ~1 M external pyridine (Fig. S23), and even more for **3d**. The effect is not just that of an increased local base concentration, however, because the mechanism changes between the systems with external and internal pyridines, as described below.

Table 1. Second-order rate constants ($M^{-1}s^{-1}$; S.D. ≤ ±10%) and KIEs[a)] for the reactions of complexes 3a-e with different oxidants at 25 °C.

Complex (pK_a)[b)]	Oxidant (E^o) [c)]			
	$[Fe((MeO)_2bpy)_3]^{3+}$ (0.36V)	**$[Fe(Me_2bpy)_3]^{3+}$ (0.51V)**	**$[Fe(bpy)_3]^{3+}$ (0.66V)**	**$[Ru(Me_2bpy)_3]^{3+}$ (0.73V)**
3a (9.55)	1.09×10^4 (KIE = 0.38)	2.96×10^4	5.65×10^5 (KIE = 0.88)	1.62×10^6 (KIE = 2.4)
3b (9.93)	4.85×10^4 (KIE = 0.31)	6.94×10^4	6.70×10^5 (KIE = 0.99)	2.71×10^6 (KIE = 1.2)
3c (12.53)	2.26×10^7 (KIE = 0.14)	6.92×10^7	5.44×10^7 (KIE = 0.19)	7.15×10^7 (KIE = 0.28)
3d (13.32)	1.06×10^8 (KIE = 0.19)	3.39×10^8	3.35×10^8	3.70×10^8
3e (14.23)	5.45×10^8	ND[d)]	ND[d)]	ND[d)]

a) for combinations when KIE was not determined the field is left blank.

b) pK_a of the conjugate acid of the corresponding pyridine derivative residue in CH_3CN[22,37,38].

c) $M^{3+/2+}$ reduction potentials in CH_3CN versus Fc^+/Fc[22].

d) Not determined, because of the limited time resolution in the stopped-flow measurement.

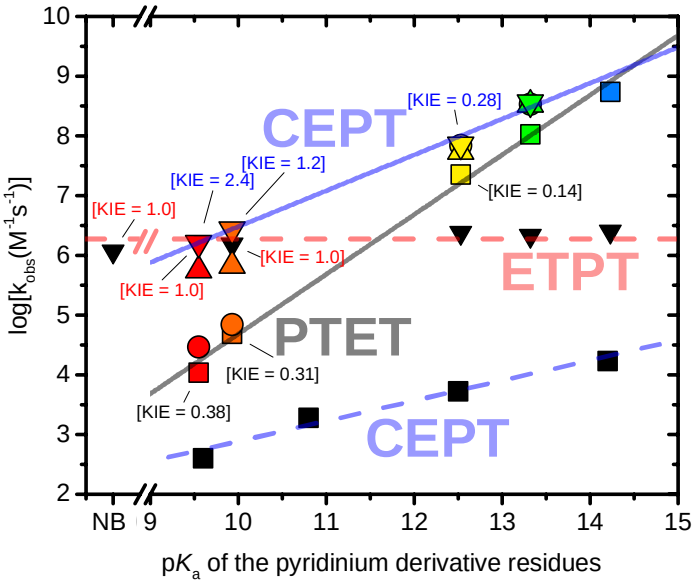

Figure 5. Dependence of the observed second-order PCET rate constant on the pK_a value of the pyridinium derivative residue, [37,38] for compounds **3a-e** (colored symbols) and for the reference complex [CpWH(CO)$_3$] (black symbols) with 7.5 equiv. external pyridine derivatives ("NB" = no pyridine added). [22] The lines show linear fits to the data with the weakest and the strongest oxidant, for **3a-e** (solid lines) and [CpWH(CO)$_3$] (dashed lines); the lines are labeled with our mechanistic assignment: concerted (CEPT) or stepwise (PTET or ETPT), see main text. Oxidants used: [Fe((MeO)$_2$bpy)$_3$]$^{3+}$ (E^0=0.36 V, £, ¢), [Fe(Me$_2$bpy)$_3$]$^{3+}$ (E^0=0.51 V, ™, ˜), [Fe(bpy)$_3$]$^{3+}$ (E^0=0.66 V, r, p), [Ru(Me$_2$bpy)$_3$]$^{3+}$ (E^0=0.73 V, s, q). Data for the CEPT reactions of [CpWH(CO)$_3$] (¢) is from a previous report[22], while additional data was collected for the ETPT reactions (, , Table S3).

The reactions of **3a-e** fall into two mechanistic regimes, the first of which contains the reactions with the two weakest oxidants. With [Fe((MeO)$_2$bpy)$_3$]$^{3+}$ (colored squares), k_{obs} increases by a factor of 10 for each pK_a unit increase of the pyridine conjugate acid (Fig. 5; slope = 1.03), which strongly suggests that an initial PT pre-equilibrium operates (k_{obs} = K_{PT}×$k_{ET\text{-}a}$). The observed kinetic isotope effect (KIE = k_H/k_D), determined with the W-D analogues of **3a-e**, ranges between 0.14 and 0.38. The KIE should mainly be an equilibrium isotope effect for intramolecular proton transfer (PT-a, Fig. 2B) between [W-H···PyR] and [W$^{\bullet}$···$^{+}$HPyR]. Based on differences in zero point energy of the W-H and H$^+$-pyridine vibrations, we calculated an expected equilibrium isotope effect of ca. 0.25 (see SI), which is in good agreement with the experimental values. Analogous results are obtained with [Fe(Me$_2$bpy)$_3$]$^{3+}$ as oxidant (circles), and the mechanism can be assigned to a stepwise PTET reaction also in this case.

The reactions of the two stronger oxidants and W-Hs with weak pendant bases (**3a** or **3b**; red and orange triangles) show a distinctly different behavior. Under these conditions, the reaction follows a concerted pathway (CEPT) without the involvement of high-energy intermediates [$W^{-\cdots+}$HPyR] or [W-$H^{+\bullet}\cdots$PyR]. This assignment is made on the basis of the primary KIE of 2.4 for **3a** and $[Ru(Me_2bpy)_3]^{3+}$, which is almost 10 times larger than KIE=0.38 for the same compound with the weaker $[Fe((MeO)_2bpy)_3]^{3+}$ oxidant. A KIE > 1 is often observed for concerted PCET reactions and reflects the lower tunneling probability for the heavier deuteron[26]. Analogously, the KIE for the reaction of **3b** with stronger oxidants is 1.2, almost 4 times larger than with $[Fe((MeO)_2bpy)_3]^{3+}$. Moreover, for the data with this oxidant, the fitted line (blue solid line) shows a slope = 0.56, which is much smaller than that of a pre-equilibrium PTET reaction. Instead, the slope is similar to what is expected for the free-energy dependence of CEPT at moderate driving force, eq. 1.

However, when $[Ru(Me_2bpy)_3]^{3+}$ reacts with **3c** KIE=0.28, which means that increased basicity of the pendant group can easily turn the mechanism from CEPT to PTET. This also means that the CEPT rate constant for **3c-d** with the strong oxidant is lower than that observed, so that the slope = 0.56 of the blue solid CEPT line is an upper limit. We propose that the slope instead should be similar to that for the CEPT reaction of $[CpWH(CO)_3]$ with external pyridines (black squares, slope = 0.38)[22]. From eq. 1, and with a change of 0.059 eV per pK_a unit, the slope should be 0.51 around $\Delta G^0 = 0$, and a slope around 0.38 is expected for the range of moderate driving forces of these reactions. With the second strongest oxidant, $[Fe(bpy)_3]^{3+}$, the kinetic behavior and mechanistic assignment follows that for $[Ru(Me_2bpy)_3]^{3+}$.

Our mechanistic assignments are also consistent with the variation of k_{obs} with oxidant strength for each individual complex **3a-d** (Fig. 5, S35-40). For the complexes with stronger bases (**3c-d**), k_{obs} is almost the same for the three strongest oxidants, and only slightly smaller with the weakest one. This is expected for a PTET reaction ($k_{obs} = K_{PT} \times k_{ET\text{-}a}$) as oxidation of the anion $[(R\text{-}Cp)W(CO)_3]^-$ is exergonic enough ($-\Delta G^0_{ET\text{-}a} \geq 0.7$ eV, Table 1) that $k_{ET\text{-}a}$ is approaching the activation-less regime ($-\Delta G^0 \gg \lambda$; eq. 1) where the rate is less sensitive to further increases in driving force. For **3a-b**, the weakest oxidants give analogous results, but when the two stronger oxidants are used, k_{obs} becomes much higher because the rate of CEPT is more strongly dependent on E^0_{ox} (eq. 1) and CEPT now provides a faster reaction pathway than PTET.

Interestingly, the reaction of $[CpWH(CO)_3]$ and externally added pyridines with the same oxidant $[Ru(Me_2bpy)_3]^{3+}$ (black inverted triangles) was ET-limited ETPT, even in the presence of the strongest pyridine base used, as shown in our previous report[22]. This is seen from the fact that k_{obs} does not change when pyridines are added (red dashed line, slope = 0). For these reactions the KIE = 1.0, consistent with an ET-limited reaction. Thus, in addition to steering the mechanism by varying the strengths of oxidant and base, the intramolecular systems **3a-e** facilitate proton transfer by subtle differences in the intramolecular H-bond structure compared to the intermolecular encounter complex of $[CpWH(CO)_3]$ and the pyridines (**Table S5**). With weak oxidants (circles and squares) proton transfer is favored to an extent that PTET becomes the main mechanism for

3a-e, in contrast to the CEPT mechanism observed for the corresponding reactions with the external pyridines (black squares).

Concluding remarks

We demonstrate a large acceleration, up to more than 10^4 times, of PCET reactions in metal-hydride (M-H) complexes with pendant basic proton relays, as compared to bimolecular systems. The presence of covalently attached bases facilitates proton transfer, and alters the preferred PCET mechanism, compared to the reaction with the same pyridines as external bases. Moreover, Fig. 5 shows the distinctly different dependencies of the rate constants on the base strength for PTET (slope = 1), CEPT (slope » 0.5) and ETPT (slope = 0); corresponding differences in dependence on the oxidant strength were discussed above. With the support of KIE data, a clear assignment of the PCET mechanism under different conditions is possible. Thus, we can show here for the first time a single species reacting via all three pathways (CEPT, ETPT, PTET). This is a great illustration of the potential to tune the mechanism and the rates via enhanced PT, which is important for designing faster and more efficient catalysts of solar fuel production or fuel cells.

As our data show, a stronger oxidant or base tends to favor ETPT or PTET, respectively, whereas if both are weak CEPT often provides the fastest mechanism; the balance points in potential and basicity depends on the individual system. Facilitated proton transfer by a well-positioned base will accelerate not only CEPT but potentially also the PT-step of PTET, as illustrated by **3a-e** and the weak oxidants. Fig. 5 shows the importance of understanding the PCET mechanism under operation to optimize catalyst design, as a change in base or oxidant strength will give very different results for the different mechanisms. Our results and the underlying principles should be generally applicable to solar fuels catalysts with widely different metals and structures, as well as serve as models for interpretation of kinetic data from enzyme mutation experiments.

Methods

Synthesis of complex 3a

In glovebox, **1a** (1.06 g, 4.03 mmol, 1.0 equiv.) was sealed in a Schlenk tube. Under positive argon flow, $W(CO)_6$ (**2**, 1.42 g, 4.03 mmol, 1.0 equiv.), THF (5 mL) and DMF (10 mL) was separately added into that Schlenk tube, which was equipped with an oven-dried cold finger very quickly. Then the reaction mixture was degassed by freezing-pump-thaw for three times under positive argon. After the reaction mixture was refluxed at 130 ^{0}C for 2 hours, it was cooled down to room temperature, and DMF was removed under vacuum overnight at room temperature to yield a dark brown oily residue.

The Schlenk tube was moved into an oxygen-free wet glovebox. The oily residue was dissolved in deoxygenated NaOH aqueous solution (0.5 M, 16.10 mmol, 4.0 equiv.) to yield an orange-yellow solution. The solution was washed with degassed Et_2O for three times to remove organic impurities. After being filtered, the aqueous layer was acidified with deoxygenated acetic acid

aqueous solution (2 M) drop by drop, until pH of the mixture became about 7-8. Then the color of the mixture turned from transparent brown to milky yellow, and a dark brown oil-like organic phase was observed in the bottle of the schlenk tube. The mixture was extracted by dry degassed Et_2O for 3 times, and the organic phases were filtered and transferred into another oven-dried 100 mL Schlenk tube. The solvent of combined organic phase was removed under vacuum at room temperature, and the obtained yellow solid was extracted by pentane (40 mL, 3 times). A bright orange solid was obtained as the product after pentane was removed under vacuum, and it can be further purified by recrystallization in pentane at -35 ^{0}C (light yellow needle-like crystals, 471 mg, 23.7%).

^{1}H NMR (400 MHz, Benzene-d6, 298K): δ 8.66 (s, 1H), 7.21 (d, *J* = 6.8 Hz, 1H), 6.46 (d, *J* = 8.4 Hz, 1H), 4.89 (s, 2H), 4.52 (s, 2H), 3.30 (s, 2H), -7.09 (s, with 2 satellite peaks, $J^{183}_{W\text{-}^1H}$ = 37.6 Hz, 1H) ppm. ^{1}H NMR (400 MHz, Acetonitrile-d3, 298K): δ 8.84 (s, 1H), 8.01 (m, 1H), 7.46 (m, 1H), 5.72 (t, *J* = 2.4 Hz, 2H), 5.49 (t, *J* = 2.4 Hz, 2H), 3.97 (s, 2H), -7.30 (s, with 2 satellite peaks, $J^{183}_{W\text{-}^1H}$ = 37.6 Hz, 1H) ppm. ^{13}C NMR (100 MHz, Benzene-d6, 298K): δ 163.13 (q, *J* = 2 Hz), 146.15 (q, *J* = 4 Hz), 133.44 (q, *J* = 4 Hz), 124.58 (q, *J* = 32 Hz), 123.98 (q, *J* = 271 Hz), 122.04, 109.51, 89.62, 87.27, 36.76 ppm. ^{19}F NMR (376 MHz, Benzene-d6, 298K): δ -62.18 (s, 3F) ppm. IR (ACN, 298K): 2018.14 (ν_{co}), 1821.72 (ν_{co}) cm^{-1}. LR-ESI-MS: observed negative ion mode LR-ESI-MS spectra ([M-H]$^-$, $C_{15}H_9F_3N_1O_3W_1$, *m/z* (%)): 490.0 (79.7%), 491.0 (55.9%), 492.0 (100.0%), 493.0 (14.9%), 494.0 (86.6%), 495.0 (13.9%). HR-ESI-MS: observed negative ion mode HR-ESI-MS spectra ([M-H]$^-$, $C_{15}H_9F_3N_1O_3W_1$, *m/z):* 490.00115, 491.00345, 492.00396, 493.00723, 494.00713, 495.01049; calculated negative ion mode HR-ESI-MS spectra ([M-H]$^-$, $C_{15}H_9F_3N_1O_3W_1$, *m/z):* 490.00111, 491.00342, 492.00407, 493.00719, 494.00732, 495.01053. Element Analysis (EA): Anal. Calcd. For $C_{15}H_{10}N_1O_3W_1$, C, 36.54; H, 2.04; N, 2.84; F, 11.56; W, 37.28. Found: C, 36.41; H, 2.13; N, 3.04; F, 11.25; W, 37.03.

Complexes **3b-3e** were synthesized under the same procedure. Their detailed synthetic procedures and characterization, including NMR, IR, LR-ESI-MS, HR-ESI-MS, EA, X-ray metrics, cyclic voltammograms and details of their computational studies are given in the Supplementary Information.

Kinetic measurements of the oxidation of complex 3

Oxidation (ET or PCET) of complex **3** was examined at 25 ^{0}C using a Hi-Tech Scientific SF-51 stopped-flow set-up equipped with a halogen light source, a monochromator, a 0.2 cm quartz cell and a photomultiplier detector connected to an oscilloscope. All the solutions of complexes **3** should be the freshly prepared in a glovebox under Ar atmosphere. The solutions of the oxidants were prepared through exhaustive electrolysis of the corresponding reduced species at a required concentration in 0.1 M Bu_4NPF_6/CH_3CN in the glovebox under Ar atmosphere. A large-surface-area platinum grid was used as the working electrode and, the platinum counter electrode was separated from the bulk solution by a glass frit. Then the solutions of both reactants were

transferred with gas-tight syringes to the inert gas chamber of the stopped-flow spectrofluorimeter as soon as possible, for the measurement of kinetic traces under positive argon flow. Inside the inert gas chamber, silicon gel was used as both the desiccant and blue humidity indicator. Every rate constant was received after 5 to 7 repeats, and its uncertainty (s.d.) has been estimated less than 10%.

Methods of purification quality control of the chemicals, typical time traces, along with fitted plots and residuals, are given in the Supplementary Information.

References and Notes:

1 Gray, H. B. Powering the planet with solar fuel. *Nat. Chem.* **1**, 7-7 (2009).
2 Graetzel, M. Artificial photosynthesis: water cleavage into hydrogen and oxygen by visible light. *Acc. Chem. Res.* **14**, 376-384 (1981).
3 Gust, D., Moore, T. A. & Moore, A. L. Solar fuels via artificial photosynthesis. *Acc. Chem. Res.* **42**, 1890-1898 (2009).
4 Montoya, J. H. *et al.* Materials for solar fuels and chemicals. *Nat. Mater.* **16**, 70-81 (2017).
5 Faunce, T. A. *et al.* Energy and environment policy case for a global project on artificial photosynthesis. *Energy Environ. Sci.* **6**, 695-698 (2013).
6 Steele, B. C. H. & Heinzel, A. Materials for fuel-cell technologies. *Nature* **414**, 345-352 (2001).
7 Debe, M. K. Electrocatalyst approaches and challenges for automotive fuel cells. *Nature* **486**, 43-51 (2012).
8 Dempsey, J. L., Winkler, J. R. & Gray, H. B. Proton-coupled electron flow in protein redox machines. *Chem. Rev.* **110**, 7024-7039 (2010).
9 Hay, S. & Scrutton, N. S. Good vibrations in enzyme-catalysed reactions. *Nat. Chem.* **4**, 161-168 (2012).
10 Dogutan, D. K., McGuire, R. & Nocera, D. G. Electocatalytic water oxidation by cobalt(III) hangman β-octafluoro corroles. *J. Am. Chem. Soc.* **133**, 9178-9180 (2011).
11 Bediako, D. K. *et al.* Role of pendant proton relays and proton-coupled electron transfer on the hydrogen evolution reaction by nickel hangman porphyrins. *Proc. Natl. Acad. Sci. U. S. A.* **111**, 15001-15006 (2014).
12 Helm, M. L., Stewart, M. P., Bullock, R. M., DuBois, M. R. & DuBois, D. L. A Synthetic nickel electrocatalyst with a turnover frequency above 100,000 s^{-1} for H_2 Production. *Science* **333**, 863-866 (2011).
13 O ' Hagan, M. *et al.* Proton delivery and removal in $[Ni(P^R_2N^{R'}_2)_2]^{2+}$ hydrogen production and oxidation catalysts. *J. Am. Chem. Soc.* **134**, 19409-19424 (2012).
14 Zhang, S., Appel, A. M. & Bullock, R. M. Reversible heterolytic cleavage of the H–H bond by molybdenum complexes: controlling the dynamics of exchange between proton and hydride. *J. Am. Chem. Soc.* **139**, 7376-7387 (2017).
15 Costentin, C., Passard, G., Robert, M. & Savéant, J.-M. Pendant acid–base groups in molecular catalysts: H-bond promoters or proton relays? Mechanisms of the conversion of CO_2 to CO by electrogenerated iron(0)porphyrins bearing prepositioned phenol functionalities. *J. Am. Chem. Soc.* **136**, 11821-11829 (2014).
16 Lilio, A. M. *et al.* Incorporation of pendant bases into Rh(diphosphine)$_2$ complexes: synthesis, thermodynamic studies, and catalytic CO_2 hydrogenation Activity of $[Rh(P_2N_2)_2]^+$ complexes. *J. Am. Chem. Soc.* **137**, 8251-8260 (2015).
17 Seu, C. S., Appel, A. M., Doud, M. D., DuBois, D. L. & Kubiak, C. P. Formate oxidation via β-deprotonation in $[Ni(P^R_2N^{R'}_2)_2(CH_3CN)]^{2+}$ complexes . *Energy Environ. Sci.* **5**, 6480-6490 (2012).
18 Roy, S. *et al.* Molecular cobalt complexes with pendant amines for selective electrocatalytic reduction of carbon dioxide to formic acid. *J. Am. Chem. Soc.* **139**, 3685-3696 (2017).
19 Costentin, C., Drouet, S., Robert, M. & Savéant, J.-M. A local proton source enhances CO_2 electroreduction to CO by a molecular Fe catalyst. *Science* **338**, 90-94 (2012).
20 Pegis, M. L. *et al.* Homogenous electrocatalytic oxygen reduction rates correlate with reaction overpotential in acidic organic solutions. *ACS Central Science* **2**, 850-856 (2016).
21 Auer, B., Fernandez, L. E. & Hammes-Schiffer, S. Theoretical analysis of proton relays in electrochemical proton-coupled electron transfer. *J. Am. Chem. Soc.* **133**, 8282-8292 (2011).

22 Bourrez, M., Steinmetz, R., Ott, S., Gloaguen, F. & Hammarström, L. Concerted proton-coupled electron transfer from a metal-hydride complex. *Nat. Chem.* **7**, 140-145 (2015).
23 Elgrishi, N., Kurtz, D. A. & Dempsey, J. L. Reaction parameters influencing cobalt hydride formation kinetics: implications for benchmarking H_2-evolution catalysts. *J. Am. Chem. Soc.* **139**, 239-244, (2017).
24 Norskov, J. K., Bligaard, T., Rossmeisl, J. & Christensen, C. H. Towards the computational design of solid catalysts. *Nat. Chem.* **1**, 37-46 (2009).
25 Olsson, M. H. M., Siegbahn, P. E. M. & Warshel, A. Simulating large nuclear quantum mechanical corrections in hydrogen atom transfer reactions in metalloenzymes. *J. Biol. Inorg. Chem.* **9**, 96-99 (2004).
26 Hammes-Schiffer, S. & Stuchebrukhov, A. A. Theory of coupled electron and proton transfer reactions. *Chem. Rev.* **110**, 6939-6960 (2010).
27 Rhile, I. J. & Mayer, J. M. One-electron oxidation of a hydrogen-bonded phenol occurs by concerted proton-coupled electron transfer. *J. Am. Chem. Soc.* **126**, 12718-12719 (2004).
28 Markle, T. F., Rhile, I. J. & Mayer, J. M. Kinetic effects of increased proton transfer distance on proton-coupled oxidations of phenol-amines. *J. Am. Chem. Soc.* **133**, 17341-17352 (2011).
29 Zhang, M.-T., Irebo, T., Johansson, O. & Hammarström, L. Proton-coupled electron transfer from tyrosine: a strong rate dependence on intramolecular proton transfer distance. *J. Am. Chem. Soc.* **133**, 13224-13227 (2011).
30 Glover, S. D., Parada, G. A., Markle, T. F., Ott, S. & Hammarström, L. Isolating the effects of the proton tunneling distance on proton-coupled electron transfer in a series of homologous tyrosine-base model compounds. *J. Am. Chem. Soc.* **139**, 2090-2101 (2017).
31 Eigen, M. Proton transfer, acid-base catalysis, and enzymatic hydrolysis. Part I: elementary processes. *Angew. Chem. Int. Ed.* **3**, 1-19 (1964).
32 Tilset, M. & Parker, V. D. Solution homolytic bond dissociation energies of organotransition-metal hydrides. *J. Am. Chem. Soc.* **111**, 6711-6717 (1989).
33 Parker, V. D., Handoo, K. L., Roness, F. & Tilset, M. Electrode potentials and the thermodynamics of isodesmic reactions. *J. Am. Chem. Soc.* **113**, 7493-7498 (1991).
34 Ryan, O. B., Tilset, M. & Parker, V. D. Chemical and electrochemical oxidation of group 6 cyclopentadienylmetal hydrides. First estimates of 17-electron metal-hydride cation-radical thermodynamic acidities and their decomposition of 17-electron neutral radicals. *J. Am. Chem. Soc.* **112**, 2618-2626 (1990).
35 Jordan, R. F. & Norton, J. R. Kinetic and thermodynamic acidity of hydrido transition-metal complexes. 1. Periodic trends in Group VI complexes and substituent effects in osmium complexes. *J. Am. Chem. Soc.* **104**, 1255-1263 (1982).
36 Edidin, R. T., Sullivan, J. M. & Norton, J. R. Kinetic and thermodynamic acidity of hydrido transition-metal complexes. 4. Kinetic acidities toward aniline and their use in identifying proton-transfer mechanisms. *J. Am. Chem. Soc.* **109**, 3945-3953 (1987).
37 Kaljurand, I. *et al.* Extension of the self-consistent spectrophotometric basicity scale in acetonitrile to a full span of 28 pK_a units: Unification of different basicity scales. *J. Org. Chem.* **70**, 1019-1028 (2005).
38 Markle, T. F., Tronic, T. A., DiPasquale, A. G., Kaminsky, W. & Mayer, J. M. Effect of basic site substituents on concerted proton–electron transfer in hydrogen-bonded pyridyl–phenols. *J. Phys. Chem. A.* **116**, 12249-12259 (2012).
39 Marcus, R. A. & Sutin, N. Electron transfers in chemistry and biology. *Biochim. Biophys. Acta. - Rev. Bioenergetics.* **811**, 265-322 (1985).
40 Irebo, T., Zhang, M.-T., Markle, T. F., Scott, A. M. & Hammarström, L. Spanning four mechanistic regions of intramolecular proton-coupled electron transfer in a $Ru(bpy)_3^{2+}$–tyrosine complex. *J. Am. Chem. Soc.* **134**, 16247-16254 (2012).
41 Rhile, I. J. *et al.* Concerted proton−electron transfer in the oxidation of hydrogen-bonded phenols. *J. Am. Chem. Soc.* **128**, 6075-6088 (2006).
42 Meyer, T. J. & Caspar, J. V. Photochemistry of metal-metal bonds. *Chem. Rev.* **85**, 187-218 (1985).

Acknowledgments: Tianfei Liu acknowledges S. D. Glover, R. Fernandez-Teran and S. Wang for fruitful discussions. This work was supported by The Swedish Research Council (grant no. 2016-04271) and The Knut and Alice Wallenberg Foundation (grant no. 2011.0067). Correspondence and requests for materials should be addressed to L.H.

Supplementary Materials:

Materials and Methods

Figures S1-S46

Tables S1-S7

References (*43-62*)